A Journal of the Gesellschaft Deutscher Chemiker

Angewandte International Edition GDCh Chemie

www.angewandte.org

Accepted Article

Title: Absorptive hydrogen scavenging for enhanced aromatics yield during non-oxidative methane dehydroaromatization on Mo/H-ZSM-5 catalysts

Authors: Anurag Kumar, Kepeng Song, Lingmei Liu, Yu Han, and Aditya Bhan

To be cited as: *Angew. Chem. Int. Ed.* 10.1002/anie.201809433
Angew. Chem. 10.1002/ange.201809433

Link to VoR: http://dx.doi.org/10.1002/anie.201809433
http://dx.doi.org/10.1002/ange.201809433

WILEY-VCH

10.1002/anie.201809433

Absorptive hydrogen scavenging for enhanced aromatics yield during non-oxidative methane dehydroaromatization on Mo/H-ZSM-5 catalysts

Anurag Kumar[a], Kepeng Song[b], Lingmei Liu[b], Yu Han[b], Aditya Bhan[a]*

[a] Department of Chemical Engineering and Materials Science, University of Minnesota, Minneapolis, MN 55455, USA

[b] Advanced Membranes and Porous Materials Center, Physical Sciences and Engineering Division, King Abdullah University of Science and Technology (KAUST), Thuwal 23955-6900, Saudi Arabia.

*Corresponding Author: E-mail: abhan@umn.edu; Fax: (+1) 612-626-7246

Abstract

The addition of Zr metal particles to MoC_x/ZSM-5 in interpellet mixtures (2:1 weight ratio) resulted in maximum single-pass methane conversion of ~27% for dehydroaromatization at 973 K – in significant excess of the equilibrium prescribed ~10% conversion at these conditions – and a concurrent 1.4 – 5.6 fold increase in aromatic product yields due to circumvention of thermodynamic equilibrium limitations by absorptive hydrogen removal by Zr while retaining the cumulative aromatic product selectivity. The absorptive function of the polyfunctional catalyst formulation can be regenerated by thermal treatment in helium flow at 973 K yielding above equilibrium methane conversion in successive regeneration cycles. Hydrogen uptake experiments demonstrate formation of bulk $ZrH_{1.75}$ on hydrogen absorption by zirconium at 973 K. Cooperation between absorption and catalytic centers distinct in location and function enables circumvention of persistent thermodynamic challenges in non-oxidative methane dehydrogenation.

10.1002/anie.201809433

Dehydroaromatization (DHA) provides an attractive thermochemical route for CH_4 valorization in reference to indirect and oxidative routes that bring forth significant kinetic challenges in conferring high selectivity.[1,2] Non-oxidative conversion of CH_4 by pyrolysis reactions to produce aromatics (benzene; at ~70% carbon selectivity) occurs with near equilibrium yield ($6CH_4 \leftrightarrow C_6H_6 + 9H_2$; ~10% single pass conversion) on carbidic forms of Mo encapsulated in zeolites at temperatures ~950 K.[3–5] Oxidic precursors of Mo deposited in H-ZSM-5 zeolitic channels via vapor phase solid state ion exchange result in formulations that catalyze CH_4 DHA at 950 K– 973 K.[6] Formation of MoC_x clusters of 0.6 – 1.5 nm size after carburization of Mo-oxidic precursors in Mo/H-ZSM-5 catalyst and their involvement in catalytic C-H bond activation during CH_4 DHA reactions has been evidenced using spectroscopic studies.[3–9] Although the stoichiometry and coordination of MoC_x clusters is still a topic of debate, the proficiency and reduced nature of active Mo-centers is no longer debated in literature.[8,10–14] Four noteworthy publications in recent literature examine evolution and speciation of MoC_x species in CH_4 DHA [10,12,15,16], however, we make no effort to probe identity of MoC_x species in this study and instead report in-situ absorptive-hydrogen removal as a strategy to overcome thermodynamic limitations that limit single pass conversion in CH_4 DHA to ~10%. A recent report proposes that addition of Zr metal as a hydrogen absorber to MoO_x/H-ZSM-5 formulations leads to increased CH_4 conversion and aromatic yields.[17] These reports, however, do not arbitrate the effect of hydrogen acceptor function precisely as hydrogen/oxygen removal during the carburization transient of MoO_x conversion to MoC_x was not accounted for.

Here, we report that addition of Zr to pre-carburized Mo/H-ZSM-5 formulations (denoted as MoC_x/H-ZSM-5 in this work) in an interpellet mixture (2:1 weight ratio) leads to formation of ZrH_x species during CH_4 DHA at 973 K resulting in ~27% maximum single-pass CH_4 conversion

and enhanced yield of CH_4-derived hydrocarbon products at equivalent time-on-stream (TOS) because equilibrium limitations are transiently circumvented by the hydrogen-absorptive Zr function while the aromatic product selectivity is unperturbed. Thermal treatment of the Zr and MoC_x/H-ZSM-5 interpellet mixture in helium flow results in regeneration of the Zr absorbent leading to above-equilibrium CH_4 conversions in successive reaction-regeneration cycles.

X-ray absorption spectroscopy and computational chemistry studies have been reported to evidence formation of $(Mo_2O_5)^{2+}$ dimers occupying two proximate Al sites on air treatment of MoO_3 and H-ZSM-5 physical mixtures at 973 K.[4,5] Mo loadings ~ 5 wt% for H-ZSM-5 with Si:Al ~13 have been shown to cause irreversible damage to the zeolite framework leading to aluminum molybdate formation (inactive for CH_4 DHA).[8] Consequently, we use $Mo:Al_f$ ~0.25 (~3 wt% Mo loading) for H-ZSM-5 catalyst with Si:Al ~11.5 to ensure the required number of Al atom pairs are available for $(Mo_2O_5)^{2+}$ dimer formation and stabilization within zeolite channels.[18,19] Raman spectroscopy, HAADF-STEM, and chemical transients (Fig. 1 (a) – (c)) reported here exhibit evolution of catalyst structure during CH_4 DHA. Mo/H-ZSM-5 (Fig. 1(a)(ii)) showed a new band at 970 cm^{-1} as compared to MoO_3 and H-ZSM-5 physical mixture (Fig. 1(a)(i)) and 973 K air-treated H-ZSM-5 (Fig. 1(a)(iii)). This band corresponds to a stretching mode characteristic of Mo=O bonds [9] suggesting formation of $(Mo_2O_5)^{2+}$ dimers within zeolite channels after MoO_x thermal exchange at 973 K. HAAD-STEM of Mo/H-ZSM-5 (Fig. 1(b)(ii)) demonstrated that crystallinity of the zeolite framework was preserved and Mo species dispersed atomically (weak white contrast clusters (<1.5 nm) marked by black arrows) during thermal treatment. Initial carburization of Mo/H-ZSM-5 on CH_4 exposure at 973 K resulted in transient evolution of CO, CO_2, and H_2 as dominant products (Fig. 1(c)), before evolution of any hydrocarbon products, yielding ~2.44 ± 0.1 O:Mo during ~15.5 ks elucidating the stoichiometric reaction of $(Mo_2O_5)^{2+}$

dimers with CH_4 to form MoC_x clusters. Carburization transients of ~15.5 ks resulted in deposition of ~8.5 ± 1.0 C:Mo in line with ~10 C:Mo deposition reported previously for CH_4 DHA on Mo/H-ZSM-5 at ~973 K.[3,12,20,21]

The induction (carburization) period and initial increase and subsequent reduction in aromatic formation rates with TOS (Fig. 1(e)) is suggestive of a bifunctional catalytic mechanism wherein C-H bonds in CH_4 are activated on MoC_x clusters formed during carburization to form C_2H_x species which subsequently undergo oligomerization/hydrogen transfer on residual Brønsted acid sites within zeolite channels to form aromatics. Previous reports showed that unsupported molybdenum carbide catalyzed CH_4 and ethane conversion to C_2 products and ethylene respectively but did not yield aromatics whereas MoC_x/H-ZSM-5 catalyzed ethane conversion to benzene suggesting that both carbidic MoC_x sites and residual Brønsted acid sites are involved in CH_4 DHA. [22,23]^[24] Mo-based species are necessary to initiate CH_4 DHA reactions on Mo/H-ZSM-5 catalysts [22,23], therefore, we normalized product rates by total number of Mo atoms to account for all available Mo atoms resulting in the lowest possible rate. We also enumerated the concentration of free Brønsted acid sites in H-ZSM-5 (Si/Al = 11.5) via NH_3 uptake as 1.21 x 10^{-3} mol g_{cat}^{-1} which is similar to concentration of Al in the zeolite based on Si:Al ratio (1.33 x 10^{-3} mol g_{cat}^{-1}).

C_2H_x (ethane and ethylene) products were formed immediately on exposure of Mo/H-ZSM-5 to CH_4 at 973 K whereas benzene evolution was observed only after an induction period of ~0.6 ks and reached a maxima at ~15.5 ks after complete carburization of $(Mo_2O_5)^{2+}$ dimers to MoC_x (Fig. 1(c) and (d)) (C:Mo ~8.5 ± 1.0 deposited after ~15.5 ks). C_2H_x rate monotonically increased to a steady value of ~6 x 10^{-5} mol s^{-1} mol_{Mo}^{-1} whereas benzene, toluene, and naphthalene net formation rates achieved maxima of 2.70 x 10^{-4} mol s^{-1} mol_{Mo}^{-1}, 1.21 x 10^{-5} mol s^{-1} mol_{Mo}^{-1}, and

5.67 x 10^{-5} mol s^{-1} mol_{Mo}^{-1} respectively before monotonically decreasing at longer TOS (Fig. 1(d) and (e)). Forward rate of C_6H_6 formation (R_{for}) was calculated for the stoichiometric reaction of CH_4 to H_2 and C_6H_6 (equation 1) on Mo/H-ZSM-5 at 973 K using net rate of benzene formation (R_{net}) and effluent hydrogen, benzene, and CH_4 pressures in the regime (12 – 22 ks TOS) in which R_{net} was invariant. Using R_{net} ~2.7 x 10^{-4} mol s^{-1} mol_{Mo}^{-1} and η ~0.5 from equations 2 and 3 with K_{eq} = 0.0302 [4], we obtained R_{for} ~ (5.05 ± 0.09) x 10^{-4} mol s^{-1} mol_{Mo}^{-1}. The net and forward rates of benzene formation are similar to that previously reported for CH_4 DHA on Mo/H-ZSM-5 at 950 K– 973 K.[5,25,26] Mo/H-ZSM-5 showed near equilibrium conversion (~10%) at 973 K after carburization was complete at ~15.5 ks and monotonically decreased at long TOS (exceeding ~ 26 ks) (Fig. 1(e)).

$$CH_4 \leftrightarrow \frac{1}{6} C_6H_6 + \frac{3}{2} H_2 \quad (1)$$

$$\eta = \frac{P_{C_6H_6}^{\frac{1}{6}} P_{H_2}^{\frac{3}{2}}}{P_{CH_4} K_{eq}} \quad (2)$$

$$R_{for} = \frac{R_{net}}{(1-\eta)} \quad (3)$$

Catalyst deactivation with TOS can be attributed to continuous buildup of carbonaceous deposits within zeolite channels which leads to reduction in Brønsted acid sites, thus inhibiting formation of aromatics, as evidenced via chemical titration with dimethyl ether, XPS, ion-scattering spectroscopy, and FT-IR measurements.[3,4,21,22] We observed benzene and naphthalene selectivity to be ~67% and ~21% respectively at ~15 ks TOS, typical for CH_4 DHA reactions on Mo/H-ZSM-5.[6,27] Aromatic selectivity decreased at longer TOS with a concurrent increase in C_2H_x selectivity, consistent with deactivation of oligomerization acidic sites in zeolites by coke deposition.[5,21]

Hydrogen co-feed studies at different catalyst loadings (0.1 – 1.0 g Mo/H-ZSM-5) and H_2:CH_4 co-feeds (0.03 – 0.11 molar ratio) at 950 K by Bedard et al.[4] demonstrated that hydrogen does not (i) cause any irreversible structural or chemical modification to MoC_x moieties present in the catalyst and (ii) have any kinetic effect on the rate-limiting step of CH_4 DHA. Net benzene formation rates were lower in presence of hydrogen but R_{for} (equation 1) was invariant demonstrating that the abundant H_2 formed in catalyst bed limited aromatics production by enhancing the approach to equilibrium. This implies that single pass CH_4 conversion for CH_4 DHA can be enhanced by removal of hydrogen.

We performed CH_4 DHA on pre-carburized MoC_x/H-ZSZM-5 formulations at 973 K as shown in Fig. 1(f). Initially, Mo/H-ZSM-5 exhibited a transient profile for ~15.5 ks where $(Mo_2O_5)^{2+}$ dimers were carburized to MoC_x species with $O_{removed}$:Mo ~ 2.44 ± 0.1 (Table S1 and Fig. 1(f) catalyst labeled as Mo/H-ZSM-5). Subsequently, CH_4 DHA on the carburized sample (Fig. 1(f) labeled as MoC_x/H-ZSM-5) showed no induction period in aromatics formation because of the presence of catalytically active MoC_x moieties from pre-carburization. MoC_x/H-ZSM-5 formulation showed characteristics of Mo/H-ZSM-5 for CH_4 DHA after complete carburization of Mo-oxo species including (i) <10% CH_4 conversion (equilibrium conversion for $6CH_4 \leftrightarrow C_6H_6 + 9H_2$ at 973 K) that decreased with TOS, (ii) benzene, toluene, and naphthalene as major products with C_2H_x formed at < 3% carbon selectivity, (iii) steady benzene formation rate for ~6 ks that subsequently declined with TOS, and (iv) a shift in product selectivity towards C_2H_x at longer TOS (Fig. 1(f)). The R_{for} was ~ (4.92 ± 0.06) x 10^{-4} mol $s^{-1}mol_{Mo}^{-1}$. HAADF-STEM of Mo/H-ZSM-5 after ~15.5 ks CH_4 reaction (Fig. 1(b)(iii)) showed Mo containing particles with sizes >2 nm (grey arrows) and Mo containing clusters <1.5 nm where concentration of particles (likely on external zeolite surface) and clusters increases after ~150 ks CH_4 reaction (Fig. 1(b)(iv)), suggesting the

10.1002/anie.201809433

change in morphology of some Mo species from atomically dispersed to agglomerates of MoC_x on CH_4 exposure at 973 K.[28] Induction periods corresponding to carburization dynamics are avoided when initiating CH_4 DHA with pre-carburized catalyst formulations and allows for assessment of effects of a hydrogen-absorbent function on mitigating thermodynamic equilibrium limitations in CH_4 DHA.

Physical mixtures of Zr metal and MoC_x/ZSM-5 were constituted in an inert environment to avoid oxidation of MoC_x species due to their oxophilic nature.[4,11] CH_4 flow over Zr particles at ~973 K did not yield any products (Fig. S4). Interpellet mixtures (2:1 weight ratio) of Zr metal and MoC_x/H-ZSM-5 CH_4 DHA catalyst showed maximum single-pass CH_4 conversion ~27% due to alleviation of thermodynamic equilibrium constraints (~10% equilibrium conversion) (Fig. 2(a)). Benzene, toluene, and naphthalene were major aromatic products observed (> 92% carbon selectivity) with xylenes, C_{10}^+, and C_2H_x (ethane and ethylene) as minor products with < 6% carbon selectivity. CH_4 conversion, benzene, toluene, and naphthalene formation rates increased monotonically to ~27% at ~1.2 ks, ~5.21 x 10^{-4} mol s^{-1} mol_{Mo}^{-1} at ~1.2 ks, ~2.84 x 10^{-5} mol s^{-1} mol_{Mo}^{-1} at ~1.8 ks, and ~1.27 x 10^{-4} mol s^{-1} mol_{Mo}^{-1} at ~0.5 ks, respectively, before decreasing with TOS accompanied by a concomitant increase in C_2H_x formation rate to ~1.09 x 10^{-4} mol s^{-1} mol_{Mo}^{-1} at ~9 ks (Fig. S1(a)). After an initial increase for ~0.27 ks in effluent H_2 flow rate, there was a monotonic decrease in H_2 eluted for ~5.1 ks (Fig. S1(b)) despite high CH_4 conversion and aromatics formation presumably due to in-situ absorptive H_2 removal by Zr particles resulting in hydride formation. A subsequent increase in instantaneous H_2 effluent rate after ~5.1 ks despite a continuing decrease in CH_4 conversion and aromatics formation can be attributed to saturation of Zr particles with hydrogen leading to reduction in hydrogen-removal sites in catalyst bed.

10.1002/anie.201809433

Benzene, naphthalene, toluene, and C_2H_x instantaneous selectivity calculated on a carbon basis were ~60%, ~30%, ~3%, and ~2%, respectively, at ~27% CH_4 conversion at ~0.3 ks TOS. The identity and sequence of appearance of products remained unchanged for MoC_x/H-ZSM-5 and Zr + MoC_x/H-ZSM-5 suggesting that bifunctional pathways effecting CH_4 DHA were unperturbed upon Zr addition. The observed enhancement in CH_4 conversion and aromatic product rates (Fig. S2) can be explained as a consequence of in-situ H_2 removal resulting in accelerated CH_4 conversion to aromatics.

Cumulative aromatic product selectivity (defined as ratio of aromatic product formed, in moles carbon, to total products observed, in moles carbon) of CH_4 DHA is retained on Zr addition leading to enhancement of aromatic yields (benzene, naphthalene, toluene, xylenes, C_{10}^+, C_2H_x) and CH_4 turnovers (Fig. 3 and S3 and Table S1) where cumulative product yield at TOS, t, is defined as total number of moles of product formed per Mo at the end of time, t. A 2.1-fold increase in CH_4 converted with a concurrent 1.4, 1.6, 2.1, 2.1, and 5.4-fold increase in C_2H_x, benzene, naphthalene, toluene, and C_{10}^+ yields respectively (after 8.7 ks TOS, Table S1) were achieved via Zr and MoC_x/ZSM-5 interpellet mixtures as compared to MoC_x/ZSM-5. Concurrently, a 0.84x decrease in H_2 yield in reactor effluent was observed for Zr + MoC_x/ZSM-5 evidencing that Zr absorbs hydrogen (as discussed below) formed during CH_4 DHA. Catalyst deactivation evident from decreasing CH_4 conversion and product rates with TOS for Zr + MoC_x/H-ZSM-5 was faster as compared to MoC_x/H-ZSM-5 (Fig. 2 and S2) which can be a consequence of two factors: (i) gradual saturation of hydrogen-absorbing sites due to stoichiometric reduction of absorbent Zr to form a hydride and/or (ii) an increase in rate of deposition of unsaturated carbonaceous species owing to hydrogen removal leading to a reduction in available Brønsted acid sites for chain growth reactions. Our results to-date do not allow us to distinguish between these two scenarios. We

calculate ~3.46 C per Mo is deposited from a total of ~35.85 mol_{CH4} mol_{Mo}^{-1} CH_4 converted (after 8.7 ks TOS) with Zr addition (equation 4) while ~1.74 C per Mo is deposited from ~35.39 mol_{CH4} mol_{Mo}^{-1} converted (after 14.7 ks TOS) by a MoC_x/H-ZSM-5 formulation evincing the high efficiency of this polyfunctional catalyst formulation to convert CH_4 to aromatic products.

$$C_{product} = \left(2 \times C_2H_x + 6 \times C_6H_6 + 7 \times C_7H_8 + 8 \times C_8H_{10} + 10 \times C_{10}H_8 + 11 \times C_{10}^{+}\right) \quad (4)$$

The hydrogen absorption capacity of Zr metal at 973 K was determined by H_2 uptake experiments (Fig. 4 and S5 and Table S2) at different H_2 uptake pressures (3.28 – 95.13 kPa). Proportional decrease in breakthrough time and heavyside functions for uptake curves demonstrate that rate of H_2 uptake on Zr metal is not kinetically relevant and transport of H_2 from MoC_x moieties in zeolite to Zr limits bulk H_2 absorption by Zr during CH_4 DHA at 973 K. Temperature-programmed-desorption (TPD) at ~1193 K in helium flow following H_2 uptake (Fig. 4(b) and (d)) resulted in stoichiometric removal of absorbed H_2 demonstrating regeneration of Zr after H_2 absorption. These results demonstrate that (i) Zr metal absorbs H_2 at ~973 K consistently across a large H_2 pressure range (3.28 – 95.13 kPa) to form $ZrH_{1.75}$, and (ii) all absorbed hydrogen can be removed by helium TPD at ~1193 K to regenerate Zr metal. Bulk crystalline characteristics of metallic Zr and stoichiometry of Zr hydride post-hydrogen uptake were confirmed by X-ray diffraction (Fig. 4(e)).

The hydrogen-absorption function of polyfunctional Zr + MoC_x/H-ZSM-5 catalyst formulation was regenerated by treating the catalyst in helium flow at ~973 K after performing CH_4 DHA for ~3.6 ks resulting in above-equilibrium CH_4 conversions (equilibrium conversion ~10%) during each reaction-regeneration cycle (~ 22 – 15 % maximum conversion) (Fig. 2(a)). The Zr + MoC_x/H-ZSM-5 catalyst formulation consistently converted higher amounts of CH_4 (~ 10.73 –

19.8 mol mol_{Mo}^{-1}) compared to MoC_x/H-ZSM-5 (~ 8.34 mol mol_{Mo}^{-1}) at the end of each reaction cycle (Fig. 2(b) and Table S3). This regeneration protocol does not regenerate the Brønsted acid sites lost due to formation of unsaturated carbonaceous species in zeolite channels which would account for lack of complete regeneration post helium flush. Hydrogen stoichiometrically absorbed by Zr during CH_4 reaction desorbed during helium treatment at 973 K (Fig. S6).

Thermal treatment in helium flow (~0.83 cm^3 s^{-1}) at ~1193 K of Zr + MoC_x/H-ZSM-5 following CH_4 DHA reaction at 973 K for ~9 ks (Fig. S1) resulted in H_2 and CH_4 elution from the reactor (Fig. 2(c)) presumably due to hydrogen desorption from Zr hydride and hydrogen-assisted hydrogenolysis of carbonaceous species. Removal of carbon deposits from Mo/H-ZSM-5 DHA catalysts by treatment in H_2 flow post-reaction at 973 K has been previously reported.[22] The amount of hydrogen absorbed/accumulated during each CH_4 reaction on Zr + MoC_x/H-ZSM-5 (Tables S1 and S2) was calculated using equation 5. This calculation resulted in $H_{missing}$:Zr ~1.48 (Table S1) while quantification of desorbed hydrogen during post-reaction TPD resulted in H:Zr ~1.60, suggesting that all H_2 absorbed by Zr during CH_4 DHA was removed by desorption at ~1193 K. C:Mo ~ 1.69 was removed as CH_4 during TPD which was less than C:Mo ~ 3.46 deposited during reaction presumably due to the inability of hydrogen to hydrogenolyze all carbonaceous deposits.

$$H_{missing} = \left(2 \times H_2 + 4 \times C_2H_x + 6 \times C_6H_6 + 8 \times C_7H_8 + 10 \times C_8H_{10} + 8 \times C_{10}H_8 + 10 \times C_{10}^{+}\right) - (4 \times CH_4 \text{ reacted}) \quad (5)$$

In summary, a polyfunctional formulation comprising of MoC_x/H-ZSM-5 and Zr metal enhanced maximum CH_4 conversion (~27%), synthesis rates of aromatics, and benzene, naphthalene, toluene, xylene, and C_{10}^{+} product yields (1.4 – 5.4 times) as compared to MoC_x/H-

ZSM-5 due to hydrogen absorption by Zr without any deleterious effect on C_2-C_{10} product selectivity. The absorptive-hydrogen removal function could be regenerated by thermal treatment in helium at 973 K resulting in above equilibrium CH_4 conversions (~ 22 – 15%) in successive reaction-regeneration cycles. We envision that a mathematical formulation of appropriate time and length scales for kinetic, diffusive, and convective phenomena in this polyfunctional catalytic system would reveal avenues for its further improvement.

Acknowledgement

We acknowledge financial support from KAUST (OSR Ref. 3325) and Office of Basic Energy Sciences, U.S. Department of Energy (Award DE-SC0019028) and thank Dr. Seema Thakral for XRD measurements as part of Characterization Facility, University of Minnesota, which receives partial support from NSF through MRSEC program.

References

[1] J. H. Lunsford, *Catal. Today* **2000**, *63*, 165–174.

[2] J. A. Labinger, J. E. Bercaw, *Nature* **2002**, *417*, 507–514.

[3] D. Wang, J. H. Lunsford, M. P. Rosynek, *J. Catal.* **1997**, *169*, 347–358.

[4] J. Bedard, D. Y. Hong, A. Bhan, *J. Catal.* **2013**, *306*, 58–67.

[5] H. S. Lacheen, E. Iglesia, *J. Catal.* **2005**, *230*, 173–185.

[6] H. S. Lacheen, E. Iglesia, *Phys. Chem. Chem. Phys.* **2005**, *7*, 538–547.

[7] B. M. Weckhuysen, D. Wang, M. P. Rosynek, J. H. Lunsford, *J. Catal.* **1998**, *175*, 347–351.

[8] N. Kosinov, F. J. A. G. Coumans, G. Li, E. Uslamin, B. Mezari, A. S. G. Wijpkema, E. A. Pidko, E. J. M. Hensen, *J. Catal.* **2017**, *346*, 125–133.

[9] W. Li, G. D. Meitzner, R. W. Borry III, E. Iglesia, *J. Catal.* **2000**, *191*, 373–383.

[10] I. Vollmer, B. Van Der Linden, S. Ould-Chikh, A. Aguilar-Tapia, I. Yarulina, E. Abou-Hamad, Y. G. Sneider, A. I. O. Suarez, J.-L. Hazemann, F. Kapteijn, et al., *Chem. Sci.* **2018**, *9*, 4801–4807.

[11] N. Kosinov, F. J. A. G. Coumans, E. Uslamin, F. Kapteijn, E. J. M. Hensen, *Angew. Chemie Int. Ed.* **2016**, *55*, 15086–15090.

[12] N. Kosinov, A. S. G. Wijpkema, E. Uslamin, R. Rohling, F. J. A. G. Coumans, B. Mezari, A. Parastaev, A. S. Poryvaev, M. V. Fedin, E. A. Pidko, et al., *Angew. Chemie Int. Ed.* **2018**, *57*, 1016–1020.

[13] B. Li, S. Li, N. Li, H. Chen, W. Zhang, X. Bao, B. Lin, *Microporous Mesoporous Mater.* **2006**, *88*, 244–253.

[14] I. Vollmer, G. Li, I. Yarulina, N. Kosinov, E. J. Hensen, K. Houben, D. Mance, M. Baldus, J. Gascon, F. Kapteijn, *Catal. Sci. Technol.* **2018**, *8*, 916–922.

[15] J. Gao, Y. Zheng, J.-M. Jehng, Y. Tang, I. E. Wachs, S. G. Podkolzin, *Science (80-.).* **2015**, *348*, 686–690.

[16] I. Lezcano-Gonzalez, R. Oord, M. Rovezzi, P. Glatzel, S. W. Botchway, B. M. Weckhuysen, A. M. Beale, *Angew. Chemie - Int. Ed.* **2016**, *55*, 5215–5219.

[17] P. T. Tanev, D. E. Gerwien, S. Miao, A. T. Simpson, E. C. Howland, S. S. Lim, **2016**, U.S. Patent 0368836 A1.

[18] A. I. Olivos Suarez, Á. Szécsényi, E. J. M. Hensen, J. Ruiz-Martínez, E. A. Pidko, J. Gascon, A. I. Olivos-Suarez, À. Szécsényi, E. J. M. Hensen, J. Ruiz-Martinez, et al., *ACS Catal.* **2016**, *6*, 2965–2981.

[19] B. R. Goodman, K. C. Hass, W. F. Schneider, J. B. Adams, *Catal. Letters* **2000**, *68*, 85–93.

[20] Y.-H. Kim, R. W. Borry, E. Iglesia, *Microporous Mesoporous Mater.* **2000**, *35–36*, 495–509.

[21] B. M. Weckhuysen, M. P. Rosynek, J. H. Lunsford, *Catal. Letters* **1998**, *52*, 31–36.

[22] D. Wang, J. H. Lunsford, M. P. Rosynek, *Top. Catal.* **1996**, *3*, 289–297.

[23] F. Solymosi, A. Szoke, *Appl. Catal. A Gen.* **1998**, *166*, 225–235.

[24] G. Wang, C. Gao, X. Zhu, Y. Sun, C. Li, H. Shan, *ChemCatChem* **2014**, *6*, 2305–2314.

[25] F. Solymosi, J. Cserényi, A. Szöke, T. Bánsági, A. Oszkó, *J. Catal.* **1997**, *165*, 150–161.

[26] S. Liu, L. Wang, R. Ohnishi, M. Ichikawa, *J. Catal.* **1999**, *181*, 175–188.

[27] Z. Liu, M. A. Nutt, E. Iglesia, *Catal. Letters* **2002**, *81*, 271–279.

[28] C. H. L. Tempelman, X. Zhu, E. J. M. Hensen, *Chinese J. Catal.* **2015**, *36*, 829–837.

10.1002/anie.201809433

Figures and Tables

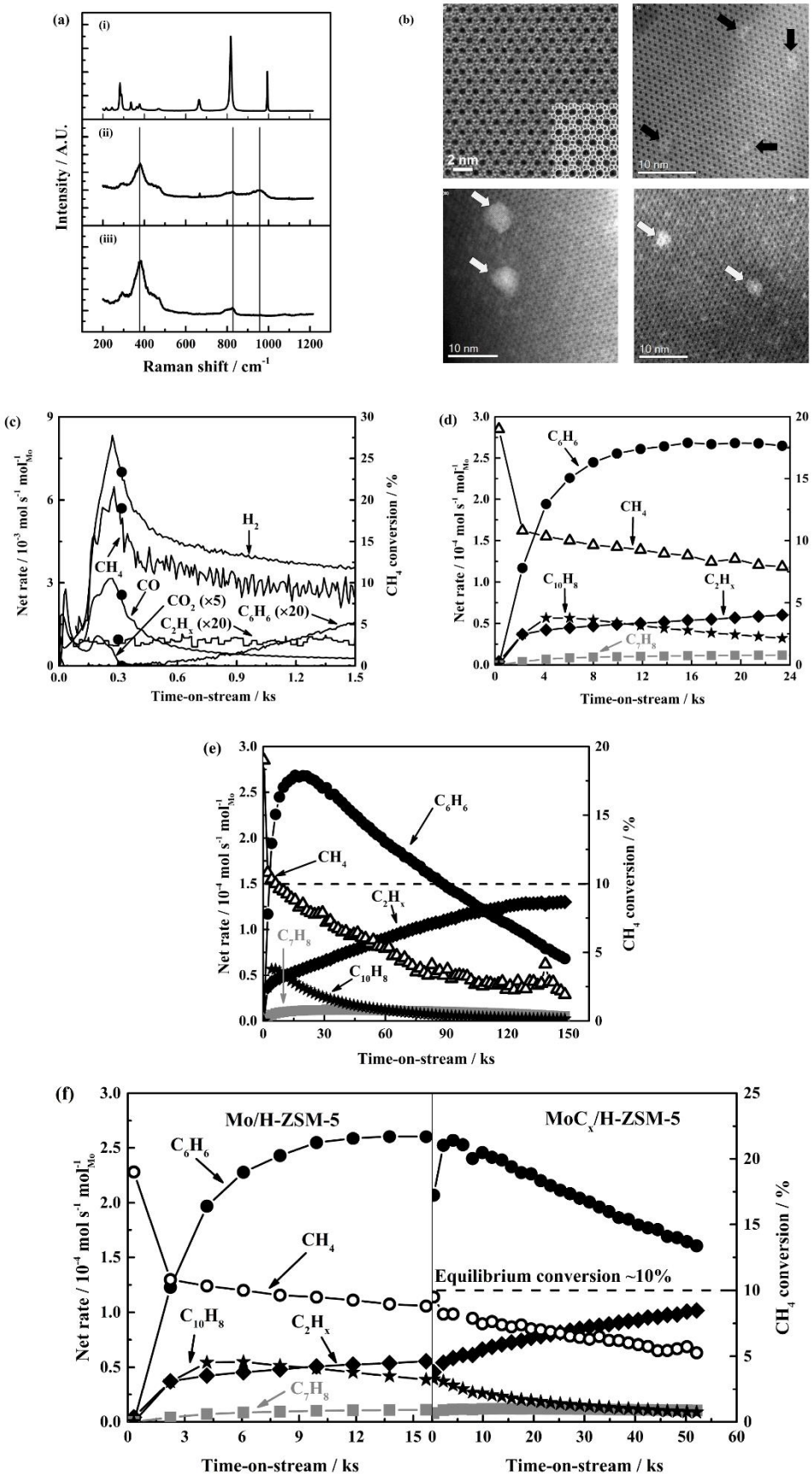

Figure 1. (a) Raman spectra of (i) MoO_3/H-ZSM-5 physical mixture, (ii) Mo/H-ZSM-5, and (iii) H-ZSM-5 air-treated at 973 K for 5 h. Lines shown as guide to eye for 376 cm^{-1}, 820 cm^{-1}, and 970 cm^{-1} bands. (b) HAADF-STEM images of (i) H-ZSM-5 along [010], (ii) Mo/H-ZSM-5 along [010], (iii) MoC_x/H-ZSM-5 along [100], and (iv) Mo/H-ZSM-5 post CH_4 reaction for ~150 ks along [100]. TOS data for (c), (d), and (e) Mo/H-ZSM-5 and (f) Mo/H-ZSM-5 and MoC_x/H-ZSM-5. (c) Symbols and lines are GC and MS data respectively. ~0.21 cm^3 s^{-1} (90 vol% CH_4), Mo/H-ZSM-5 ~1.2 g, 973 K.

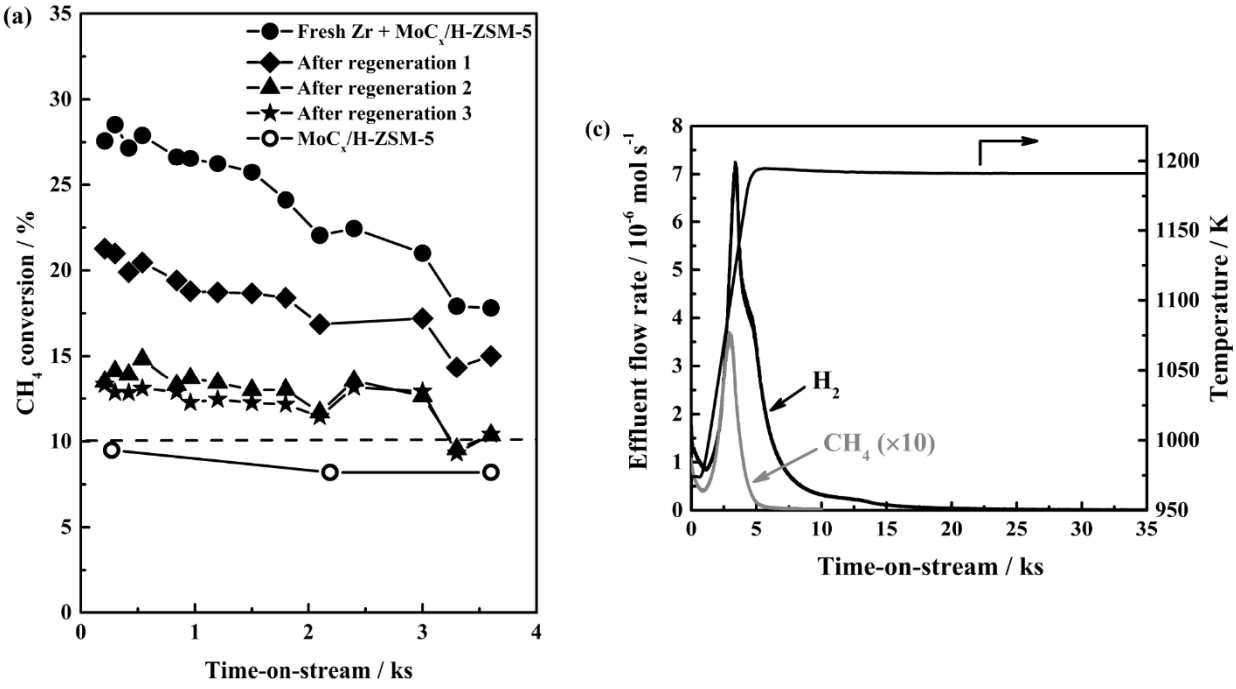

(b)

	MoC_x/H-ZSM-5	Zr + MoC_x/H-ZSM-5 Fresh	After Regeneration 1	After Regeneration 2	After Regeneration 3
CH_4 converted / mol mol_{Mo}^{-1} [a]	8.34	19.8	13.75	11.2	10.73

[a] cumulative amount after 3.6 ks TOS

Figure 2. (a) CH_4 conversion vs TOS for MoC_x/H-ZSM-5 and Zr + MoC_x/H-ZSM-5 before (fresh) and after regeneration in He flow. Regenerations 1, 2, and 3 of Zr + MoC_x/H-ZSM-5 by flushing in He flow (~0.83 cm^3 s^{-1}) at 973 K for 61.2 ks, 84.6 ks, and 34.2 ks respectively. MoC_x/H-ZSM-5 ~1.2 g, Zr ~2.4 g, ~0.21 cm^3 s^{-1} (90 vol% CH_4), ~973 K. Dashed black line indicates ~10% equilibrium conversion for $6CH_4 \leftrightarrow C_6H_6 + 9H_2$ at 973 K. (b) Cumulative CH_4 converted from data shown in (a). (c) Effluent flow rates during He TPD post-CH_4 reaction on Zr + MoC_x/H-ZSM-5 for ~9 ks (Fig. S1).

10.1002/anie.201809433

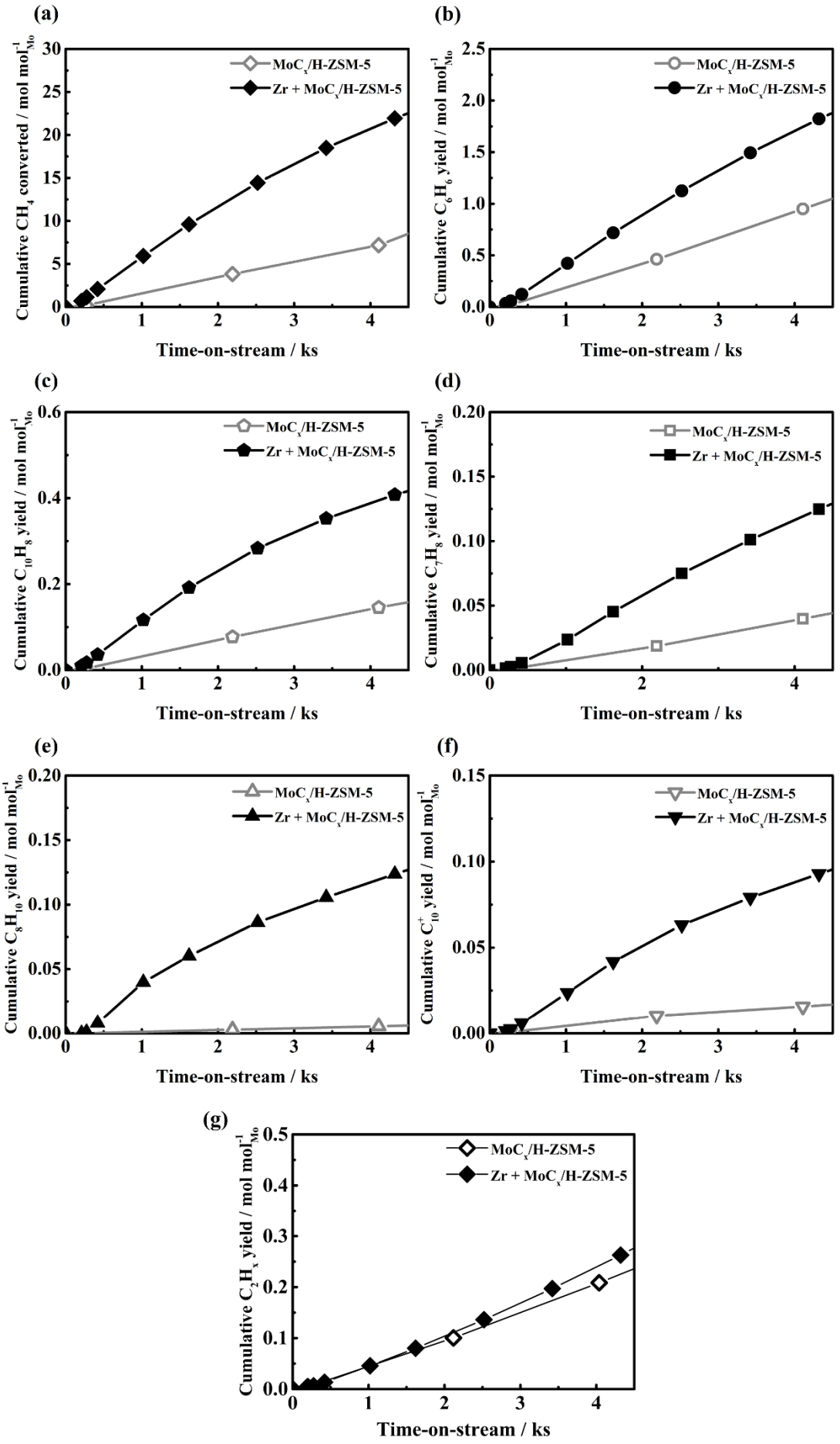

Figure 3. Cumulative (a) CH_4 converted, (b) benzene, (c) naphthalene, (d) toluene, (e) xylenes, (f) C_{10}^{+} , and (g) C_2H_x yield as a function of TOS for MoC_x/H-ZSM-5 and Zr + MoC_x/H-ZSM-5. MoC_x/H-ZSM-5 ~1.2 g, Zr ~2.4 g, ~0.21 cm^3 s^{-1} (90 vol% CH_4), reaction at ~973 K.

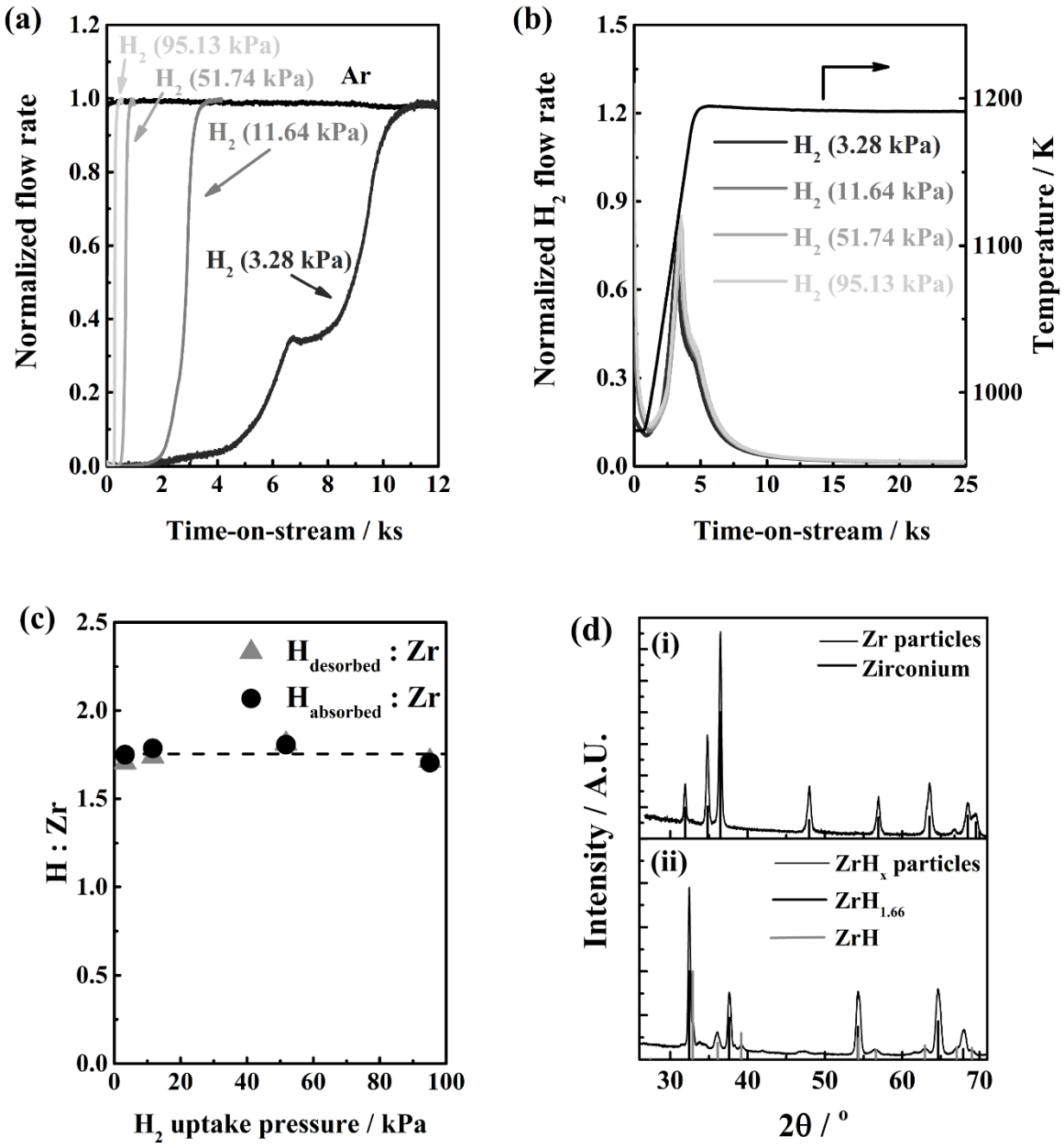

Figure 4. Normalized effluent flow rates during (a) H_2 uptake experiments for Zr and (b) helium TPD following H_2 uptake. (c) H:Zr molar ratio from H_2 uptake ($H_{absorbed}$: Zr) and helium TPD ($H_{desorbed}$: Zr). (d) XRD patterns of (i) Zr metal and (ii) Zr hydride formed by H_2 uptake of Zr. Zr ~2.4 g, Zr particle diameter ~ 3 x 10^{-4} m, feed ~1.7 cm^3 s^{-1}, H_2/Ar ~ (3.28 – 95.13) kPa/balance, ~973 K. Zr metal (JCPDS PDF # 03-065-3366), $ZrH_{1.66}$ (JCPDS PDF # 00-034-0649), and ZrH (JCPDS PDF # 00-034-0690).

10.1002/anie.201809433

Keywords: Heterogeneous catalysis, Carbides, Methane dehydroaromatization, Polyfunctional catalysis, Metal additive

Table of Contents Figure: